This document was prepared in conjunction with work accomplished under Contract No. DE-AC09-96SR18500 with the U. S. Department of Energy.

DISCLAIMER

This report was prepared as an account of work sponsored by an agency of the United States Government. Neither the United States Government nor any agency thereof, nor any of their employees, makes any warranty, express or implied, or assumes any legal liability or responsibility for the accuracy, completeness, or usefulness of any information, apparatus, product or process disclosed, or represents that its use would not infringe privately owned rights. Reference herein to any specific commercial product, process or service by trade name, trademark, manufacturer, or otherwise does not necessarily constitute or imply its endorsement, recommendation, or favoring by the United States Government or any agency thereof. The views and opinions of authors expressed herein do not necessarily state or reflect those of the United States Government or any agency thereof.

This report has been reproduced directly from the best available copy.

Available for sale to the public, in paper, from: U.S. Department of Commerce, National Technical Information Service, 5285 Port Royal Road, Springfield, VA 22161,
phone: (800) 553-6847,
fax: (703) 605-6900
email: orders@ntis.fedworld.gov
online ordering: http://www.ntis.gov/help/index.asp

Available electronically at http://www.osti.gov/bridge
Available for a processing fee to U.S. Department of Energy and its contractors, in paper, from: U.S. Department of Energy, Office of Scientific and Technical Information, P.O. Box 62, Oak Ridge, TN 37831-0062,
phone: (865)576-8401,
fax: (865)576-5728
email: reports@adonis.osti.gov

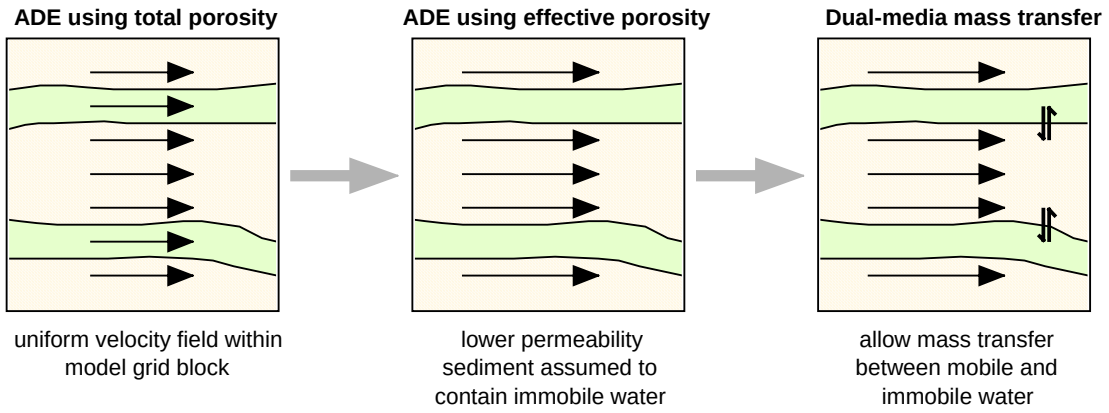

Figure 1 Conceptual development of dual-media mass transfer approach to contaminant transport modeling.

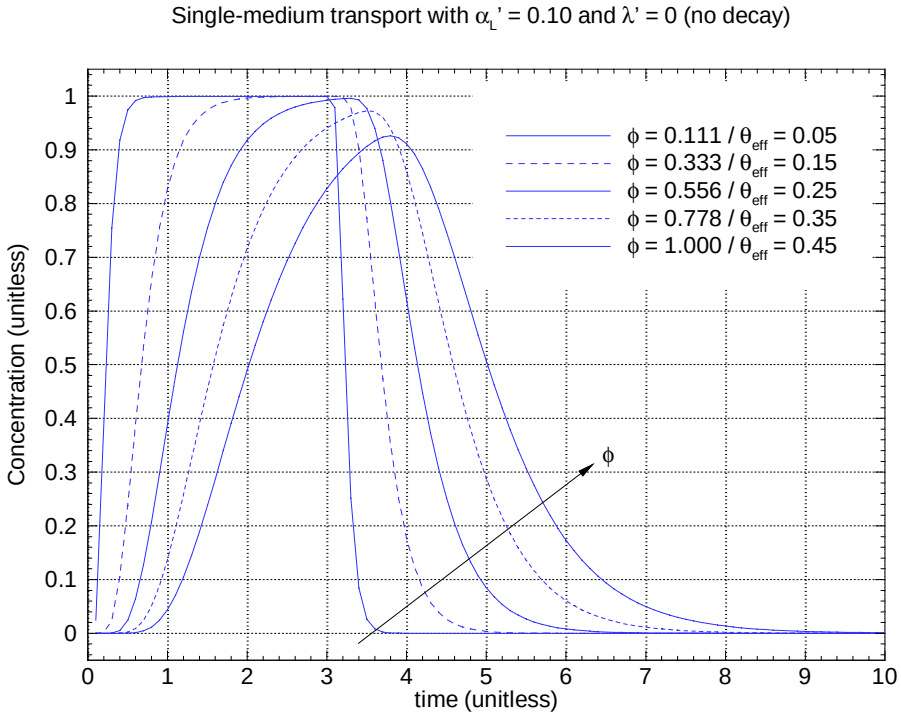

Figure 2 Non-dimensional breakthrough curves for single-medium transport, no decay and varying effective porosity.

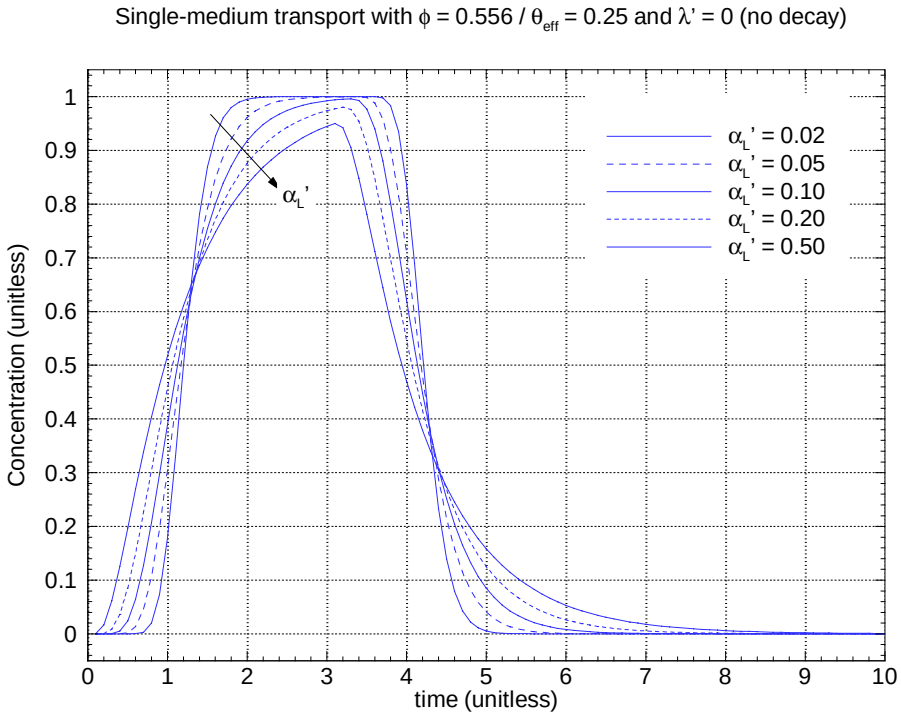

Figure 3 Non-dimensional breakthrough curves for single-medium transport, no decay and varying dispersivity.

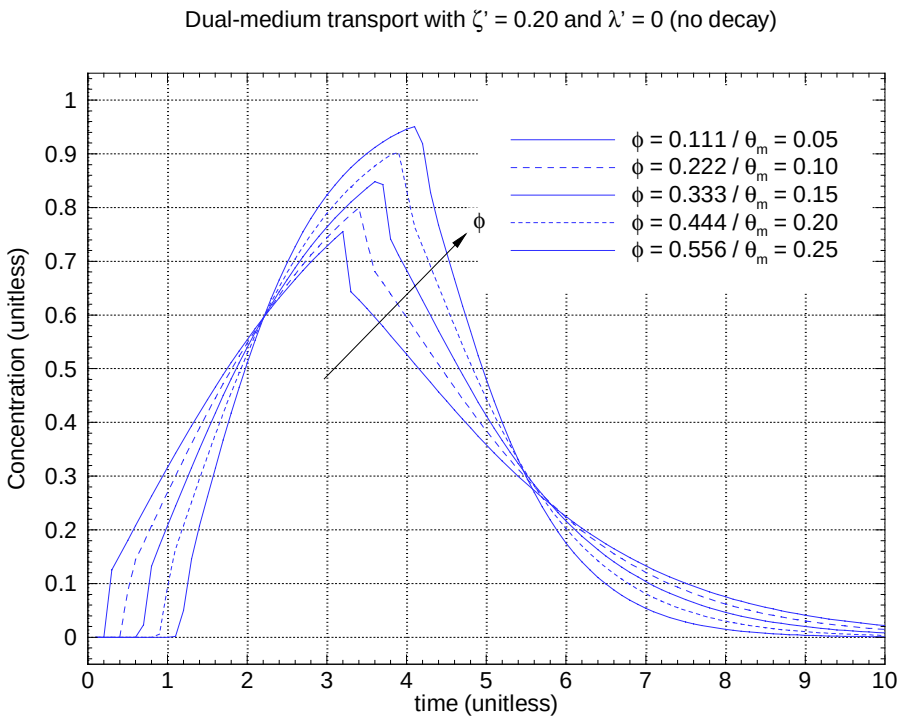

Figure 4 Non-dimensional breakthrough curves for dual-media transport, no decay and varying mobile volume fraction.

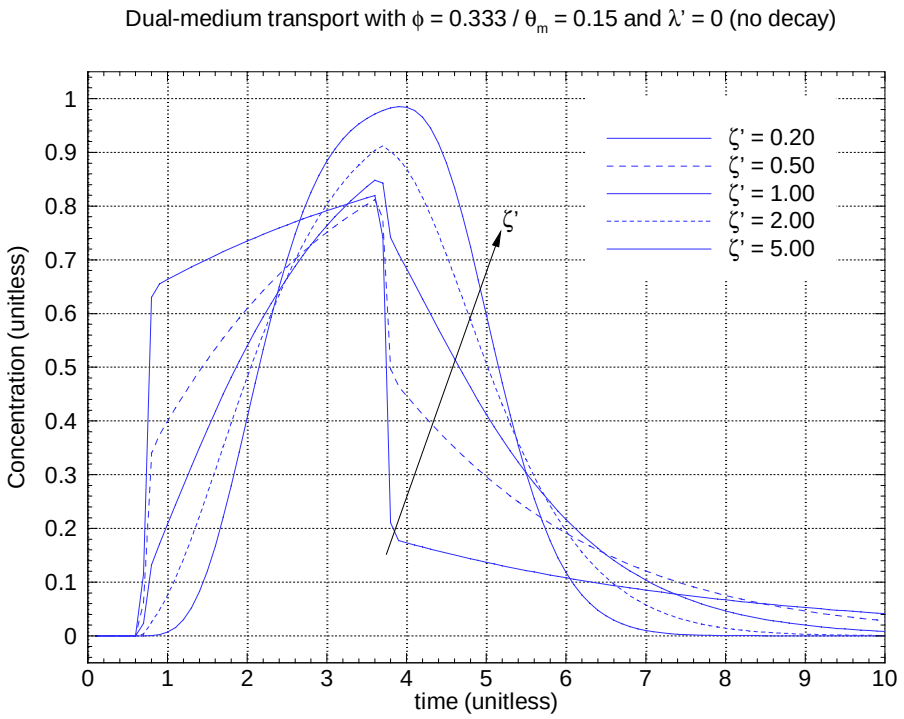

Figure 5 Non-dimensional breakthrough curves for dual-media transport, no decay and varying mass transfer coefficient.

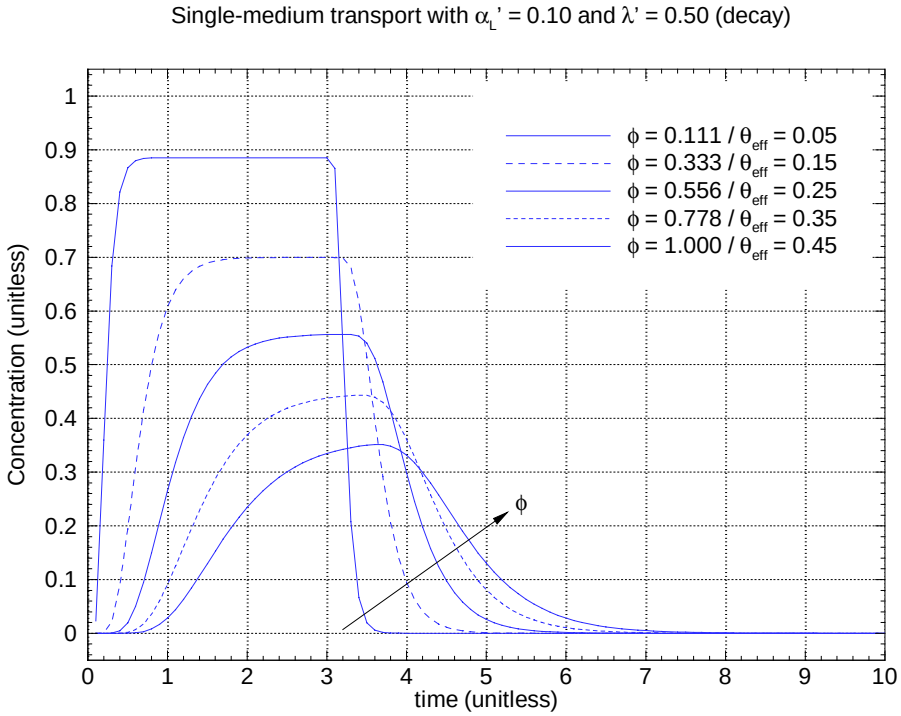

Figure 6 Non-dimensional breakthrough curves for single-medium transport, first-order decay and varying effective porosity.

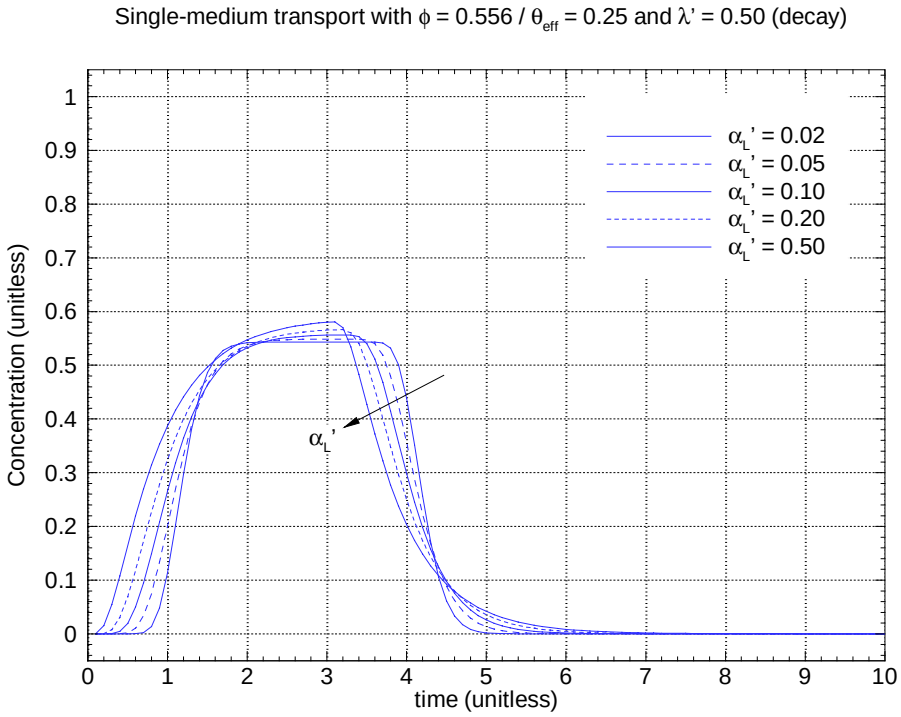

Figure 7 Non-dimensional breakthrough curves for single-medium transport, first-order decay and varying dispersivity.

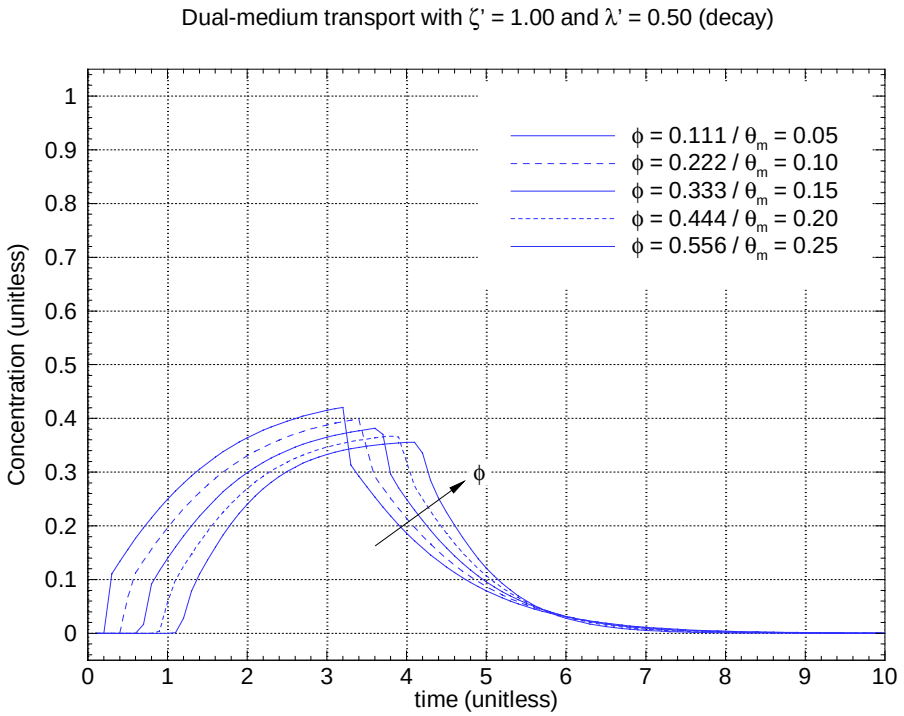

Figure 8 Non-dimensional breakthrough curves for dual-media transport, first-order decay and varying mobile volume fraction.

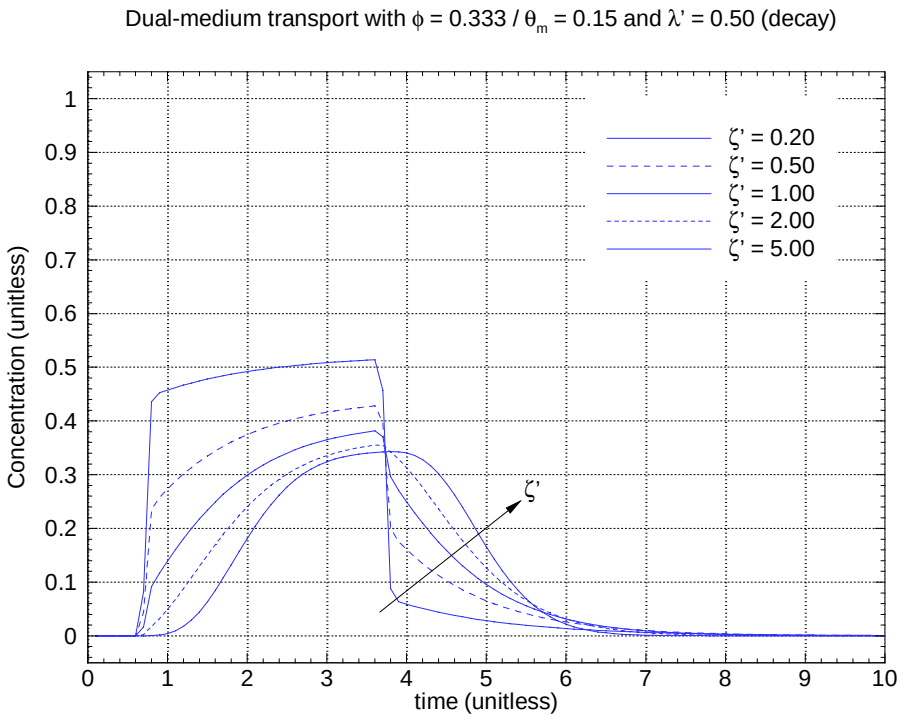

Figure 9 Non-dimensional breakthrough curves for dual-media transport, first-order decay and varying mass transfer coefficient.

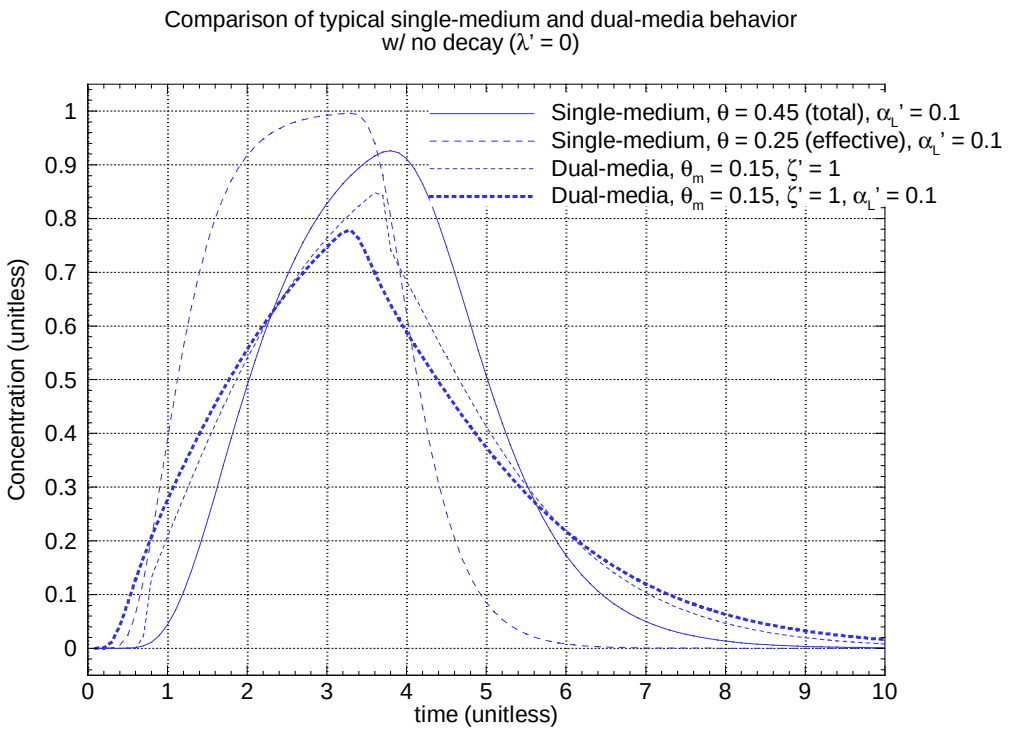

Figure 10 Comparison of single- and dual-media breakthrough with no decay and nominal parameter settings.

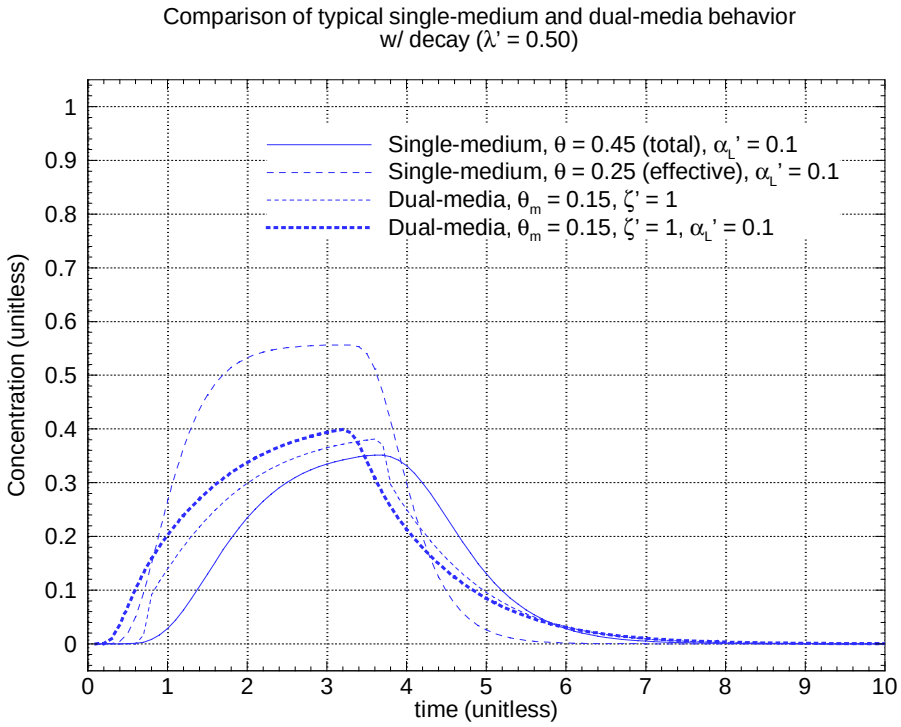

Figure 11 Comparison of single- and dual-media breakthrough with first-order decay and nominal parameter settings.

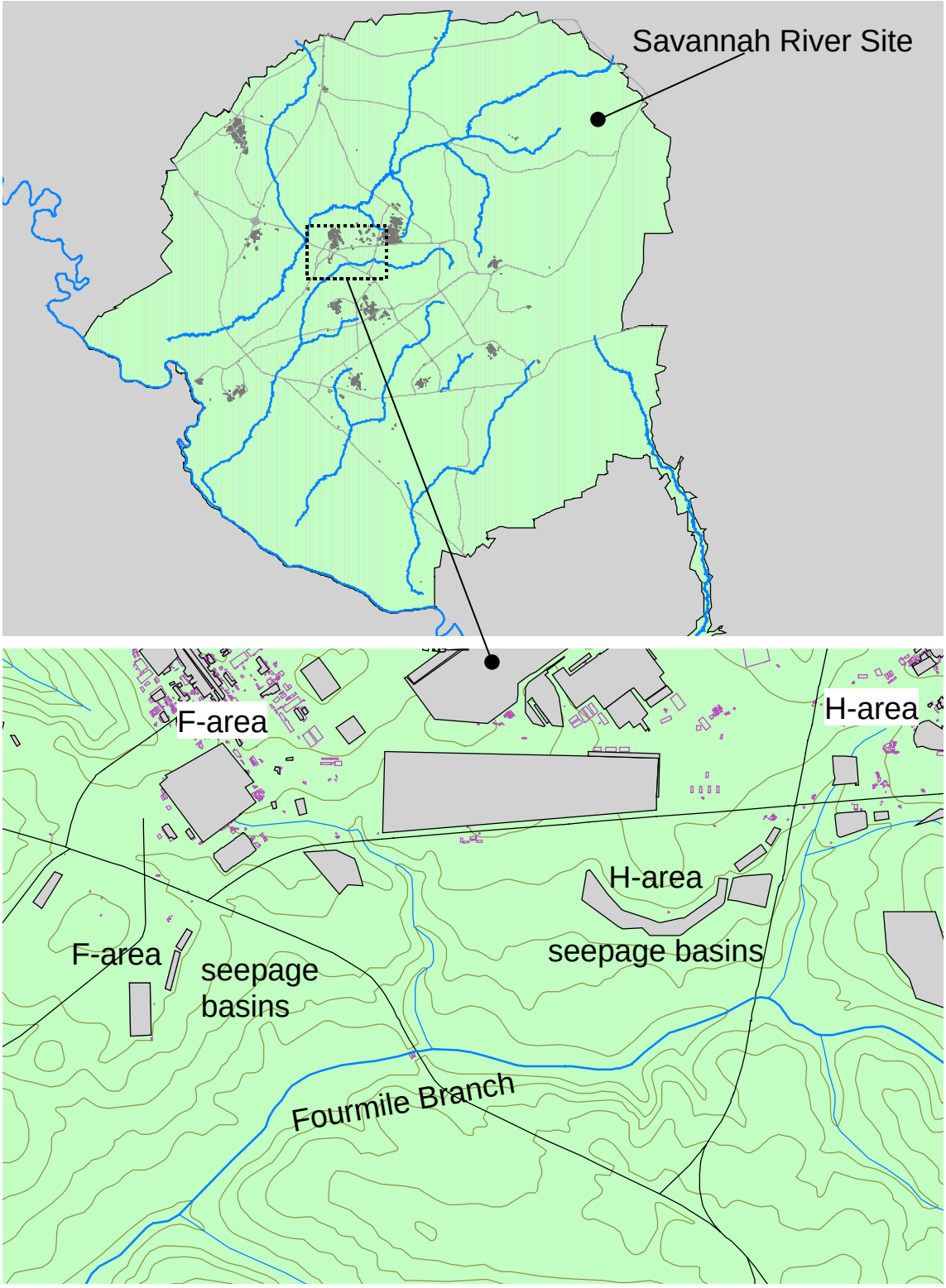

Figure 12 Location of F- and H-area seepage basins.

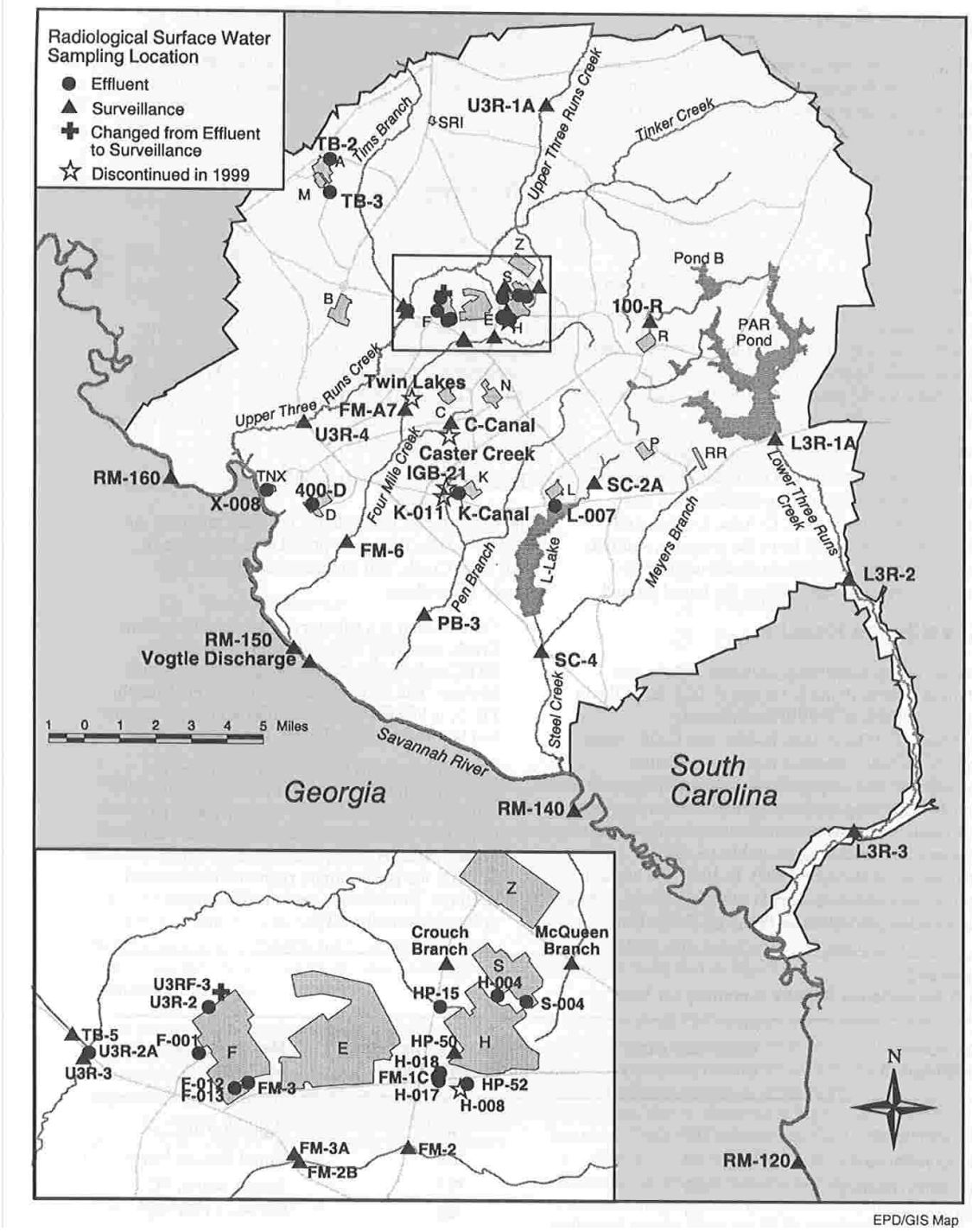

Figure 13 Environmental Protection Department surface water sampling locations; reproduced from WSRC-TR-99-00299.

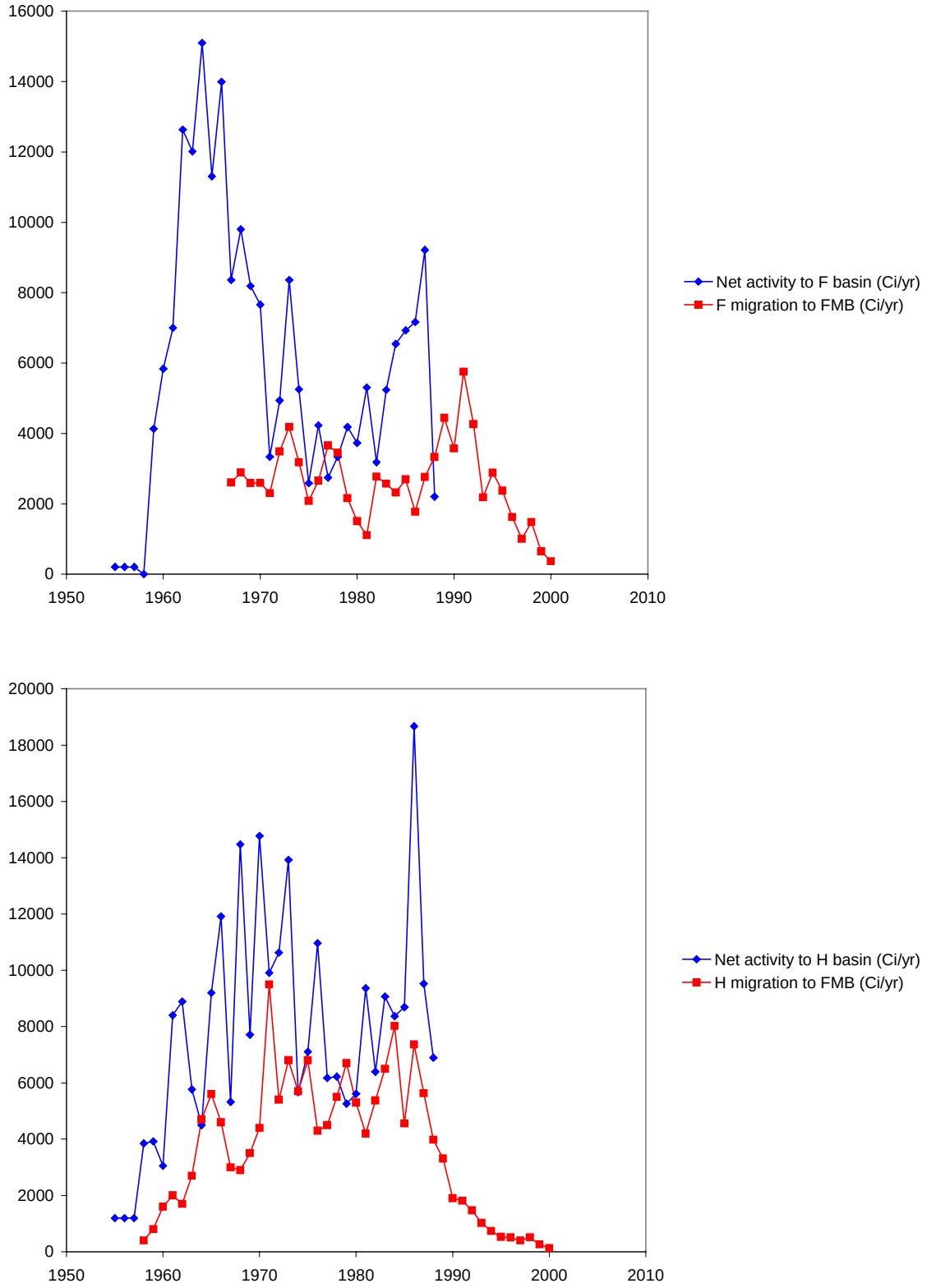

Figure 14 Tritium activity fluxes (Ci/yr) in and out of the groundwater systems associated with the F- and H-area seepage basins.

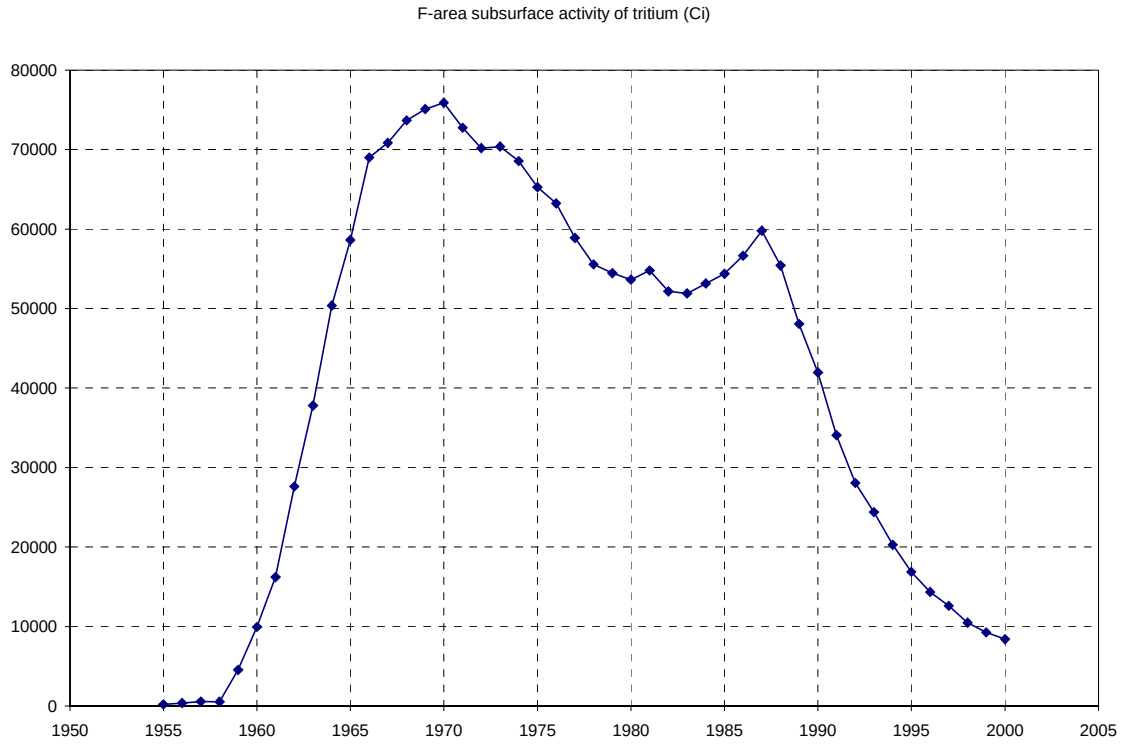

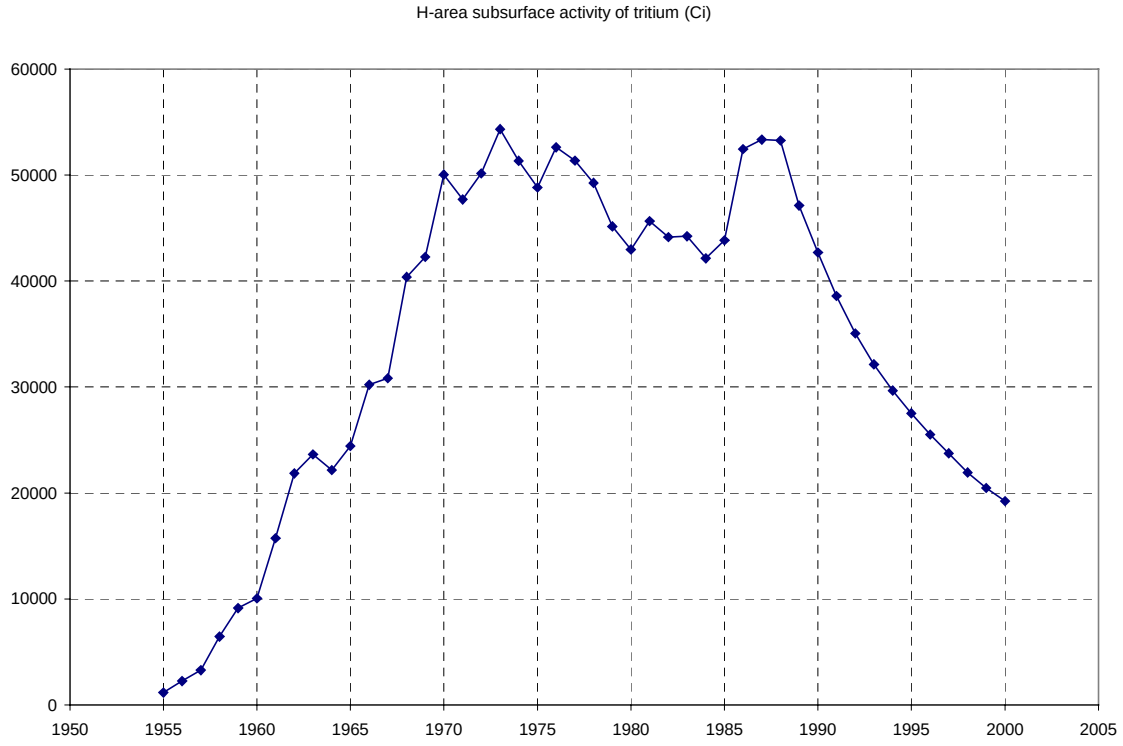

Figure 15 Tritium activity (Ci) contained within the groundwater systems associated with the F- and H-area seepage basins.

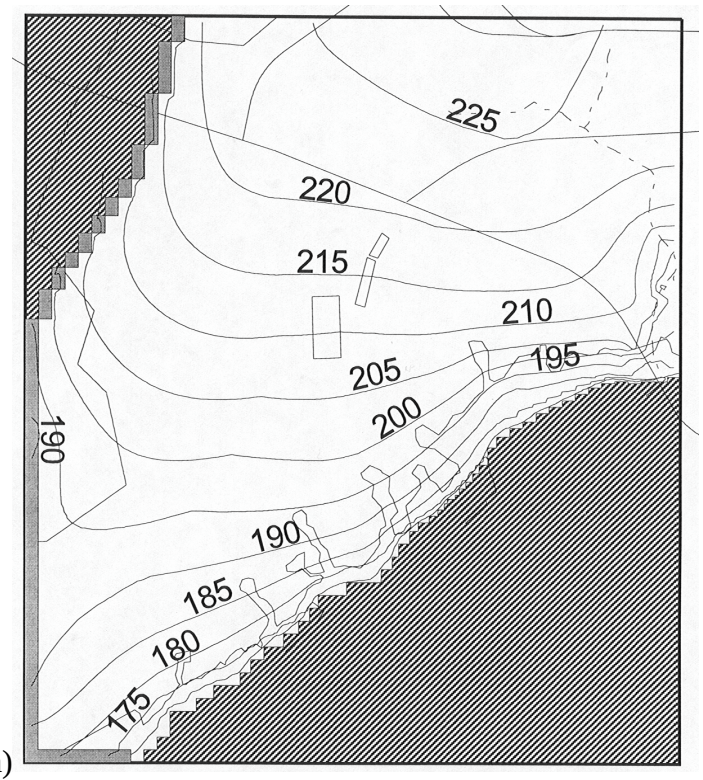

(a)

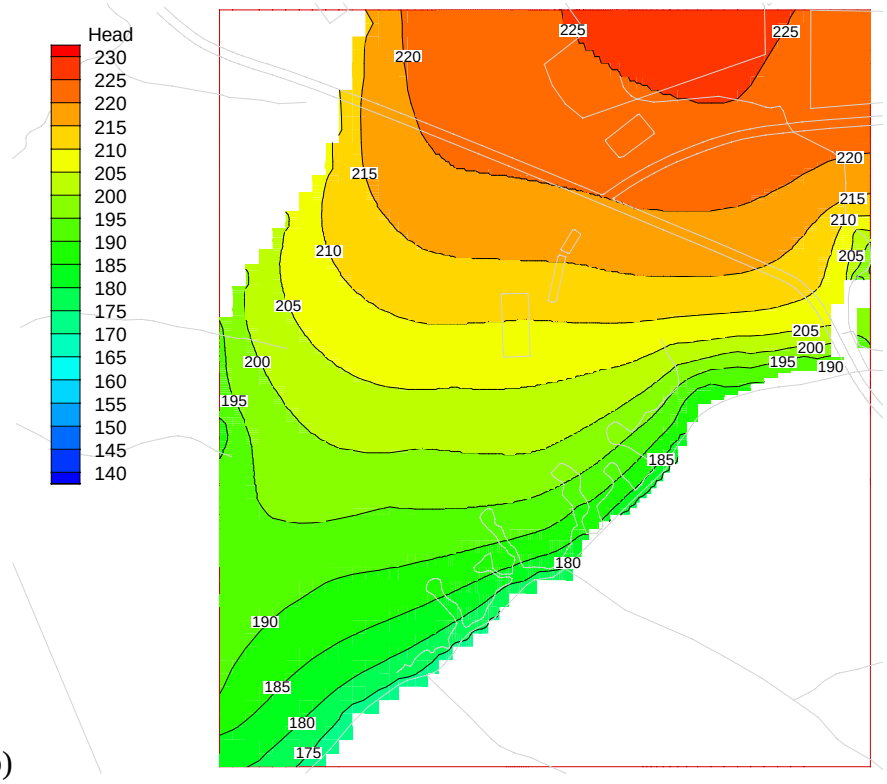

(b)

Figure 16 Comparison of simulated hydraulic head in the F-area upper aquifer zone (UAZ): a) Geotrans, b) current study.

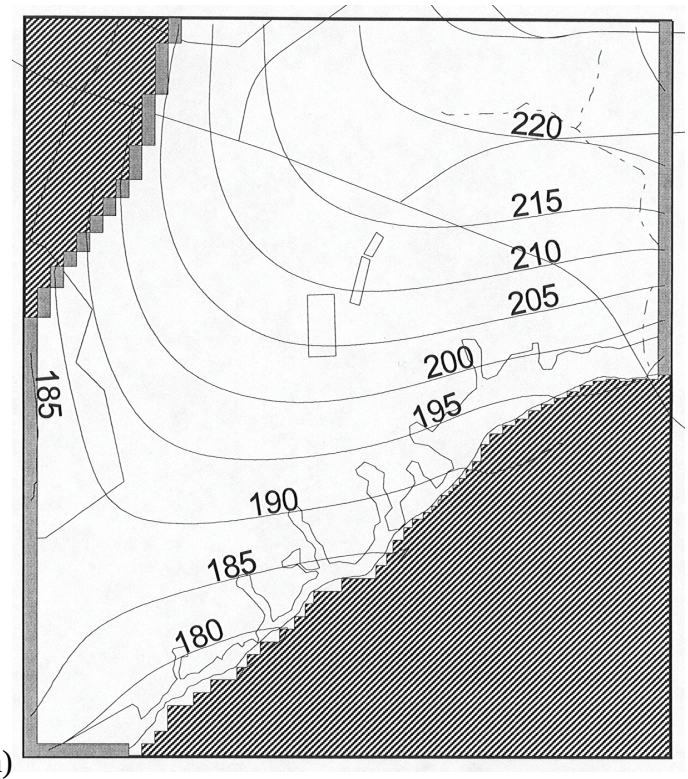

(a)

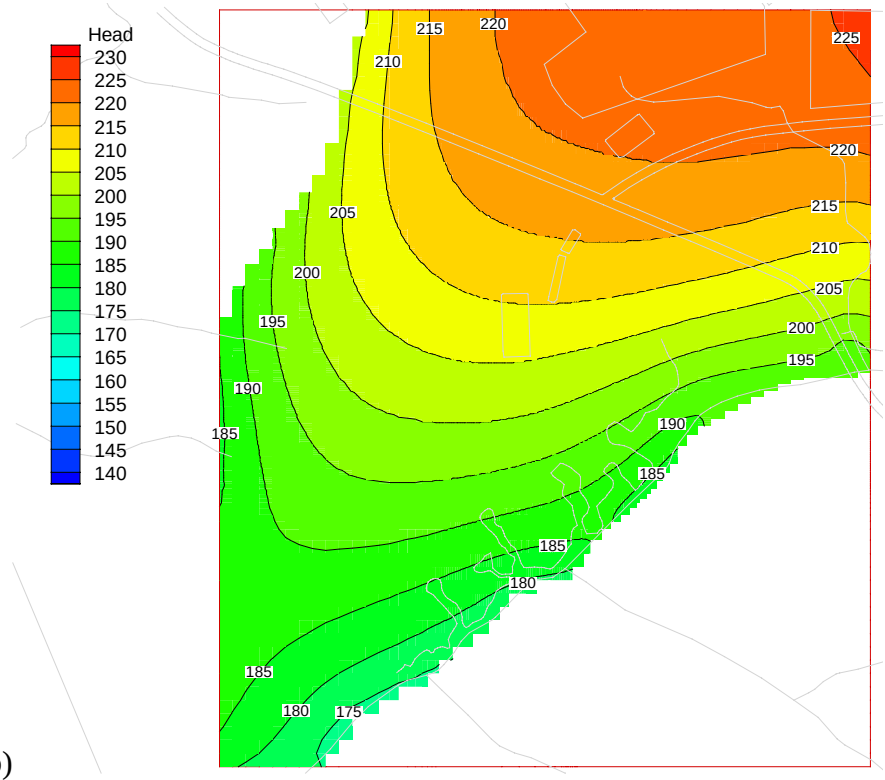

(b)

Figure 17 Comparison of simulated hydraulic head in the F-area lower aquifer zone (LAZ): a) Geotrans, b) current study.

(a)

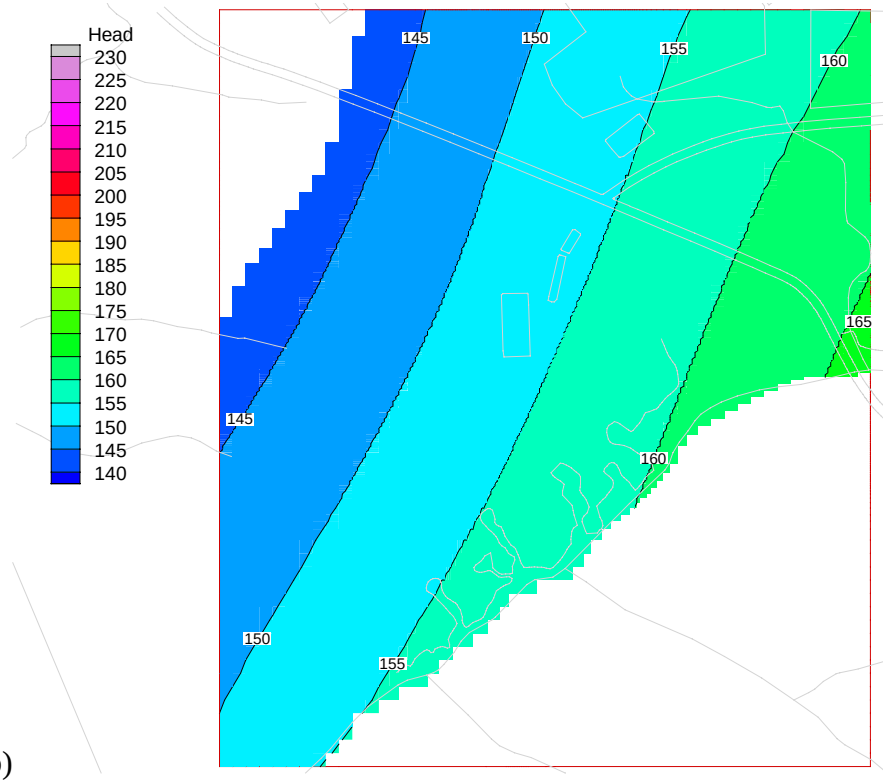

(b)

Figure 18 Comparison of simulated hydraulic head in the F-area Gordon aquifer unit (GAU): a) Geotrans, b) current study.

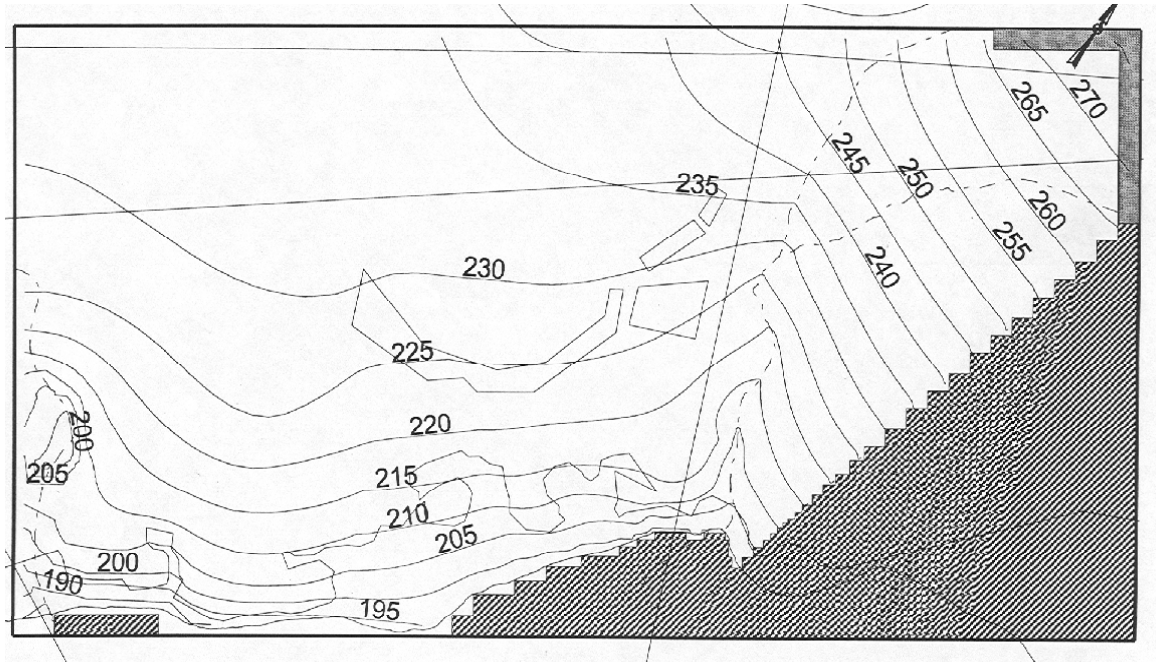

(a)

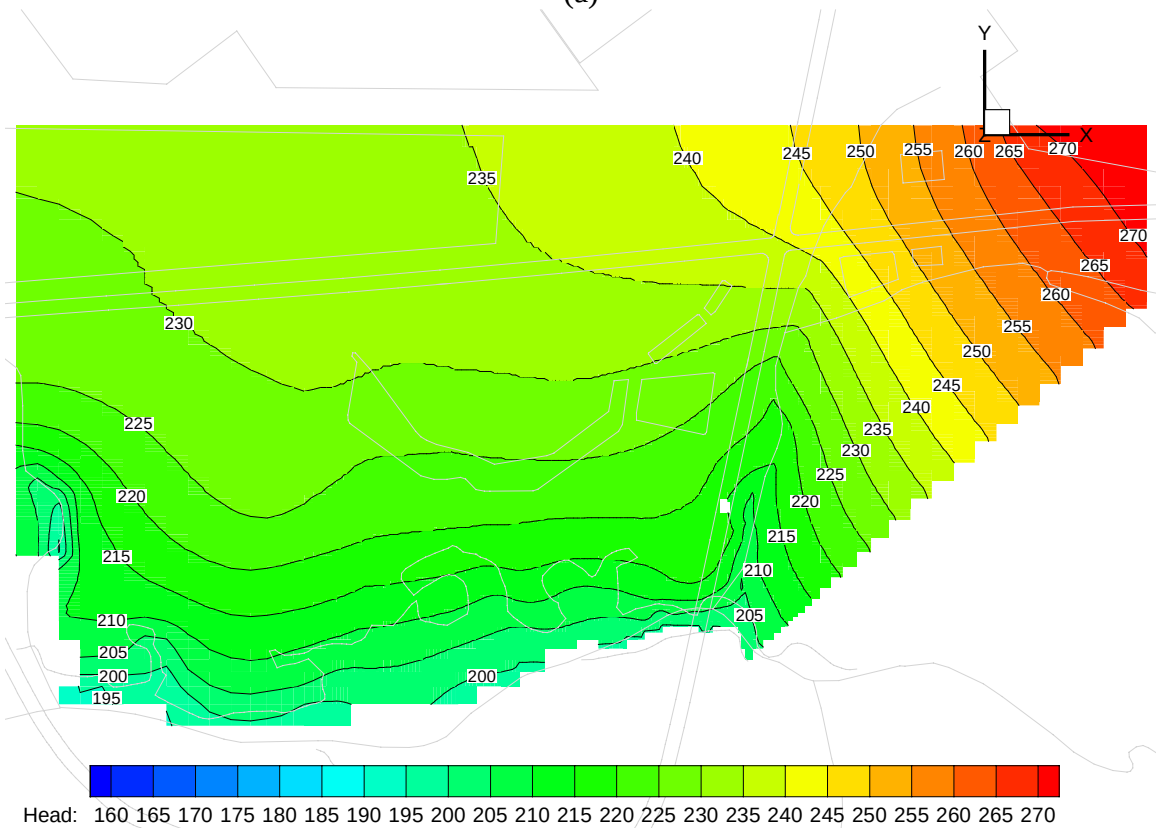

(b)

Figure 19 Comparison of simulated hydraulic head in the H-area upper aquifer zone (UAZ): a) Geotrans, b) current study.

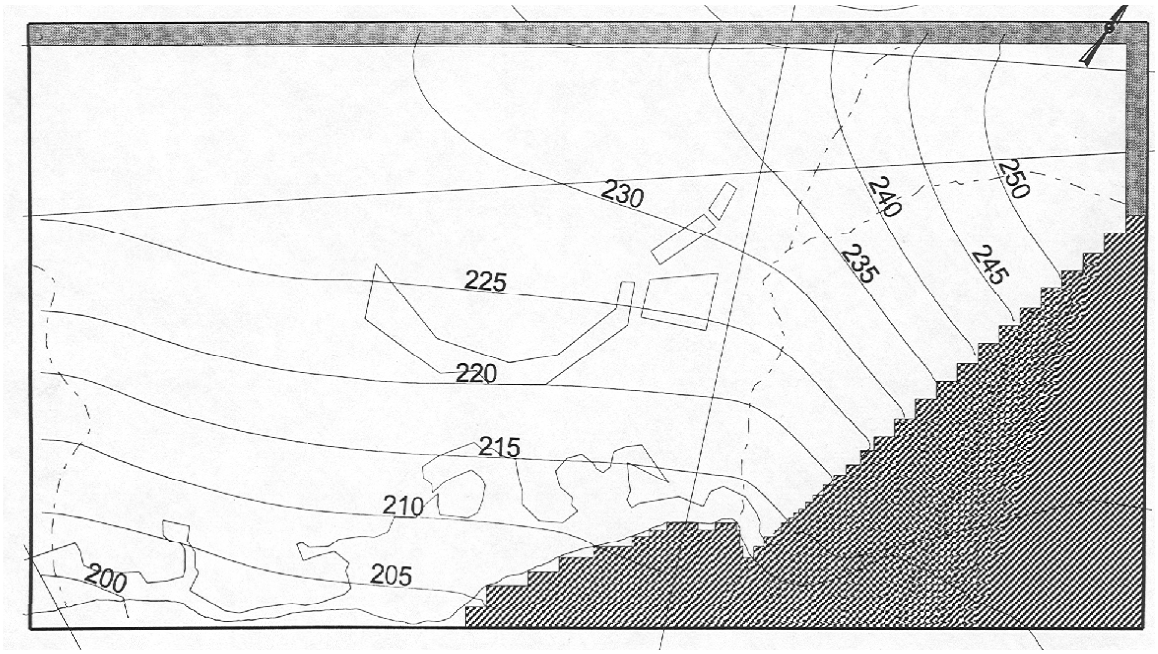

(a)

(

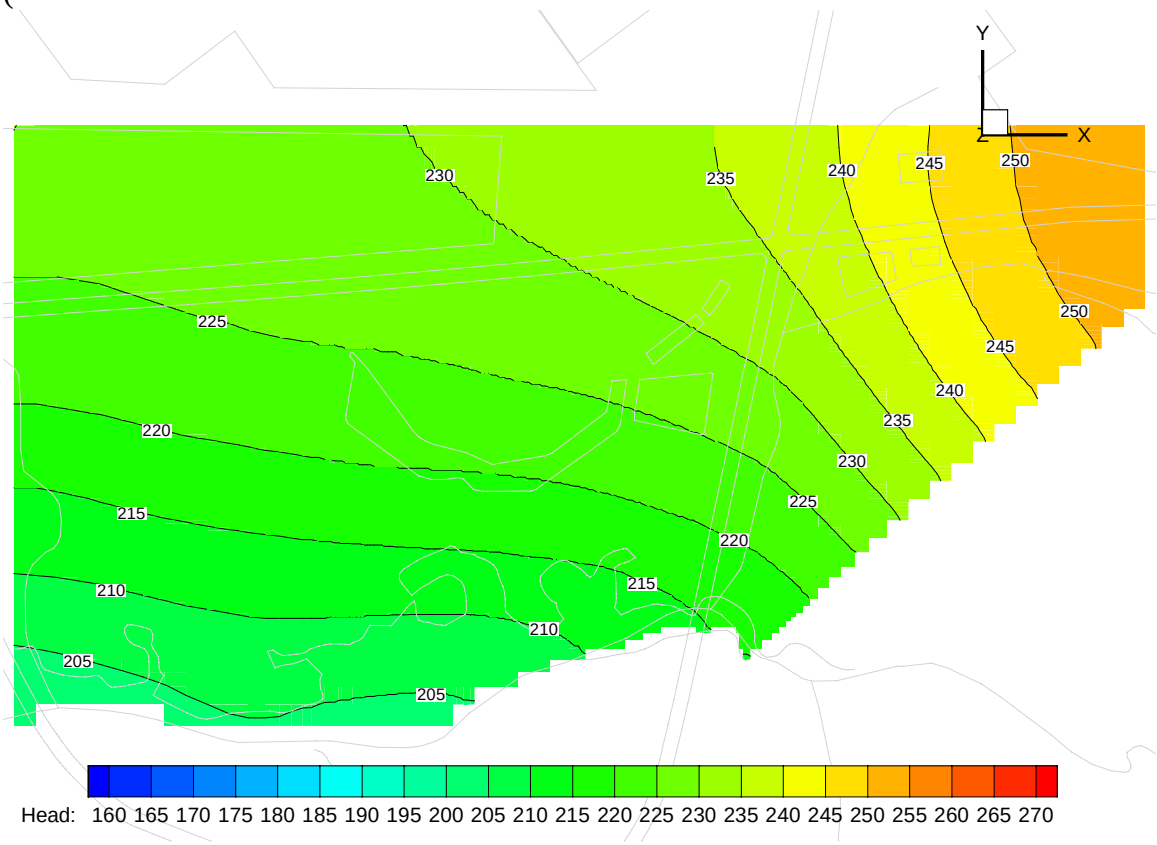

(b)

Figure 20 Comparison of simulated hydraulic head in the H-area lower aquifer zone (LAZ): a) Geotrans, b) current study.

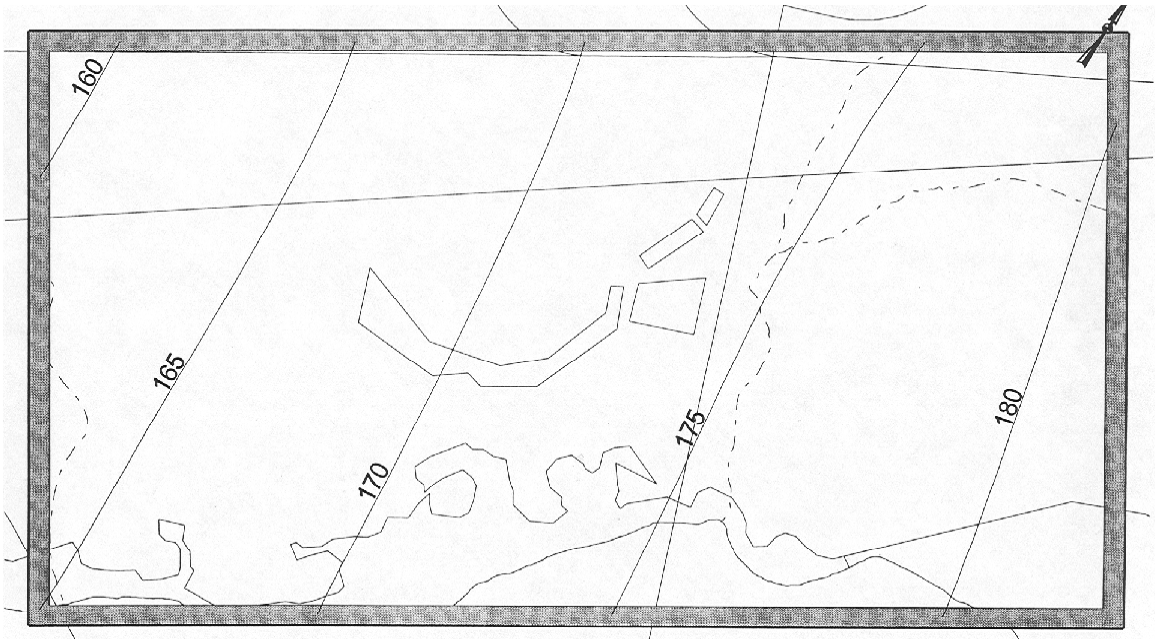

(a)

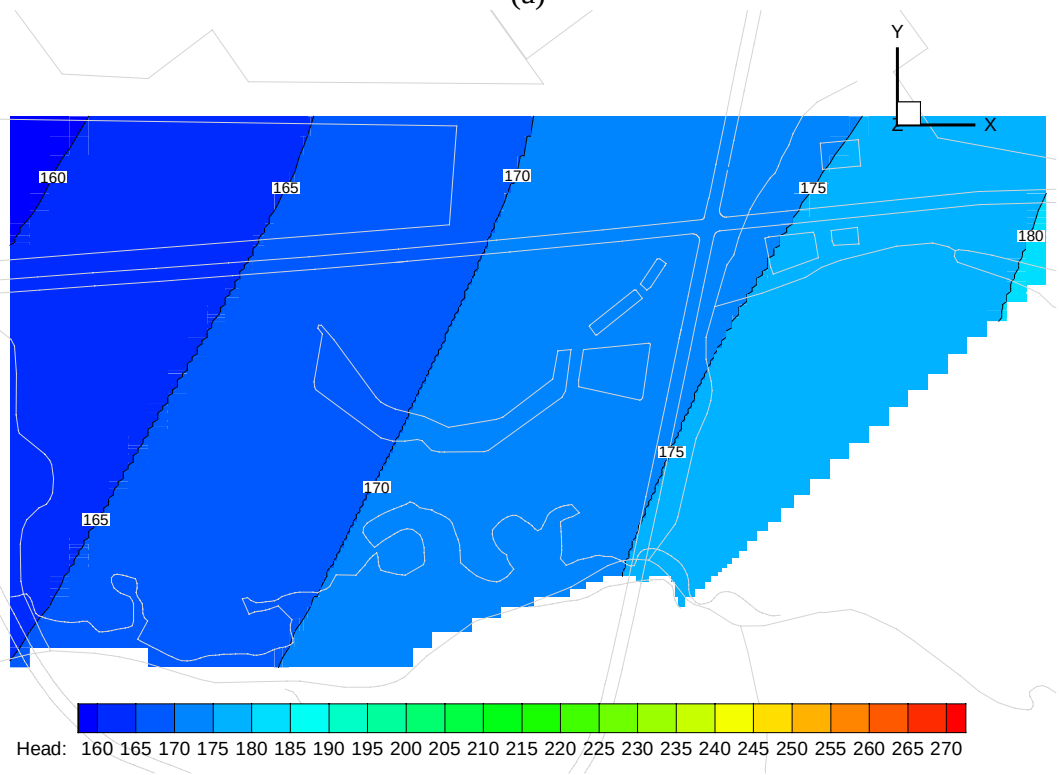

(b)

Figure 21 Comparison of simulated hydraulic head in the H-area Gordon aquifer unit (GAU): a) Geotrans, b) current study.

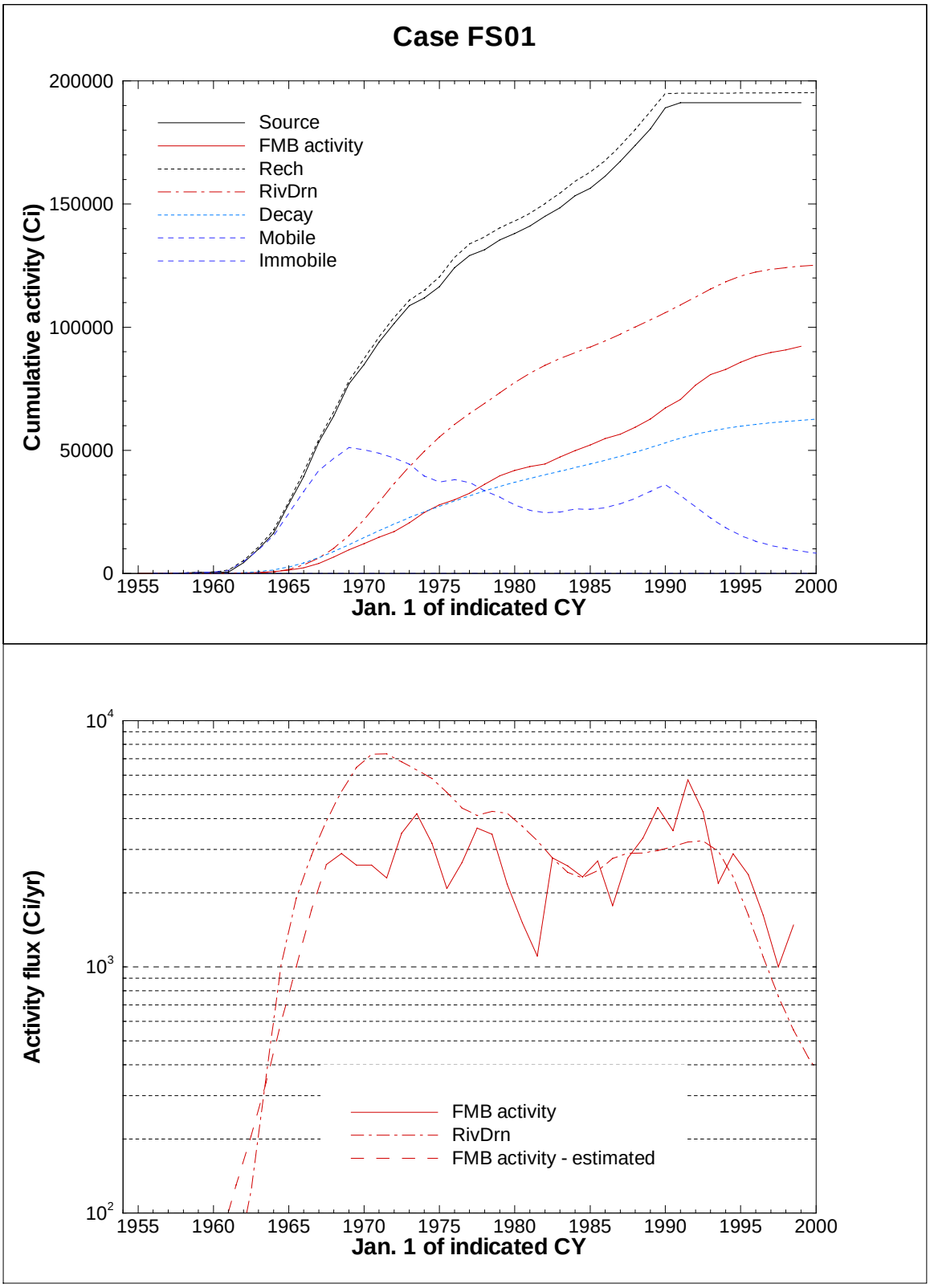

Figure 22 Example plot comparing simulated and measured cumulative activities and tritium fluxes; single-medium case FS01.

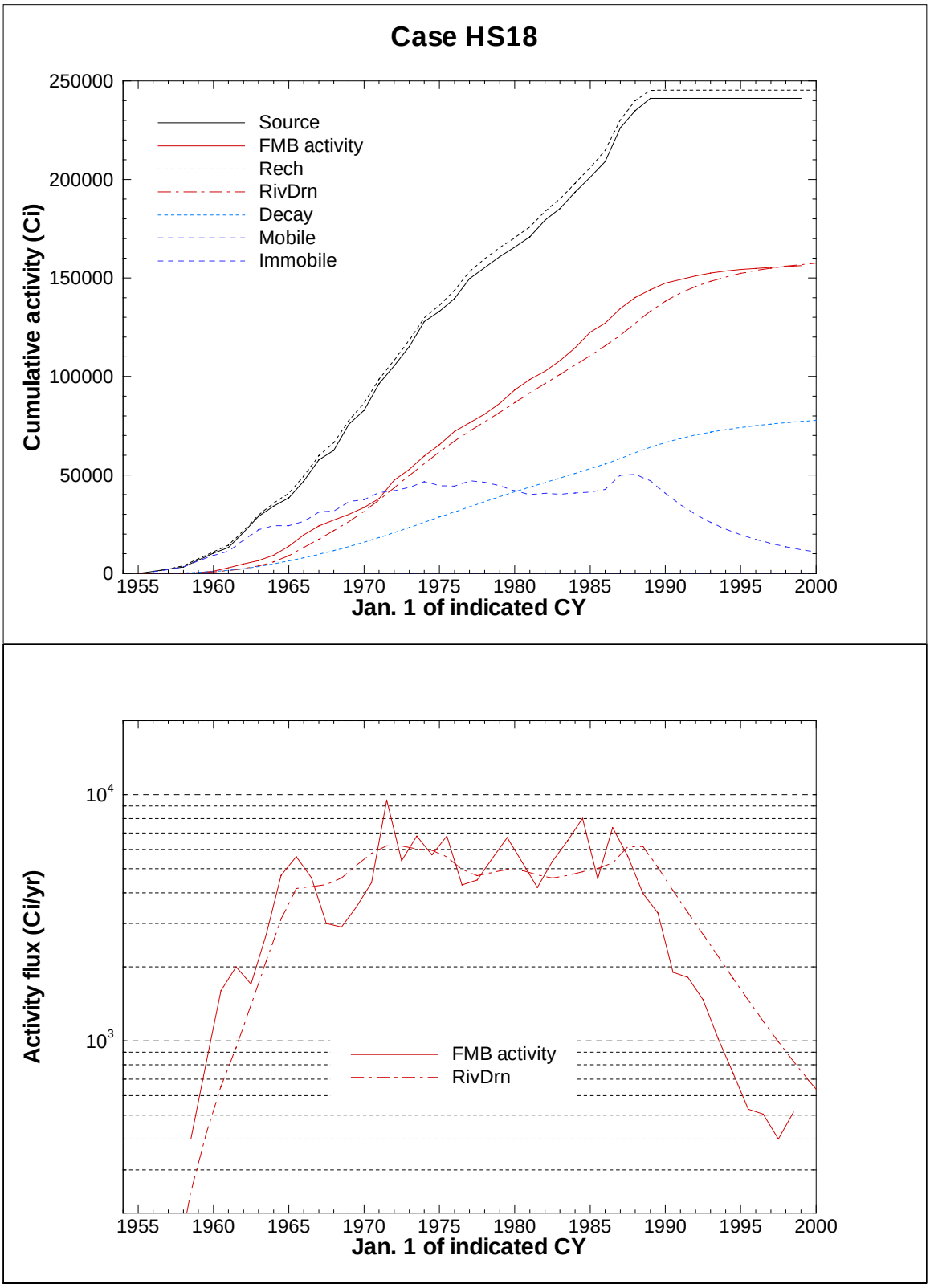

Figure 23 Calibration summary for optimal H-area single-medium transport simulation (HS-18).

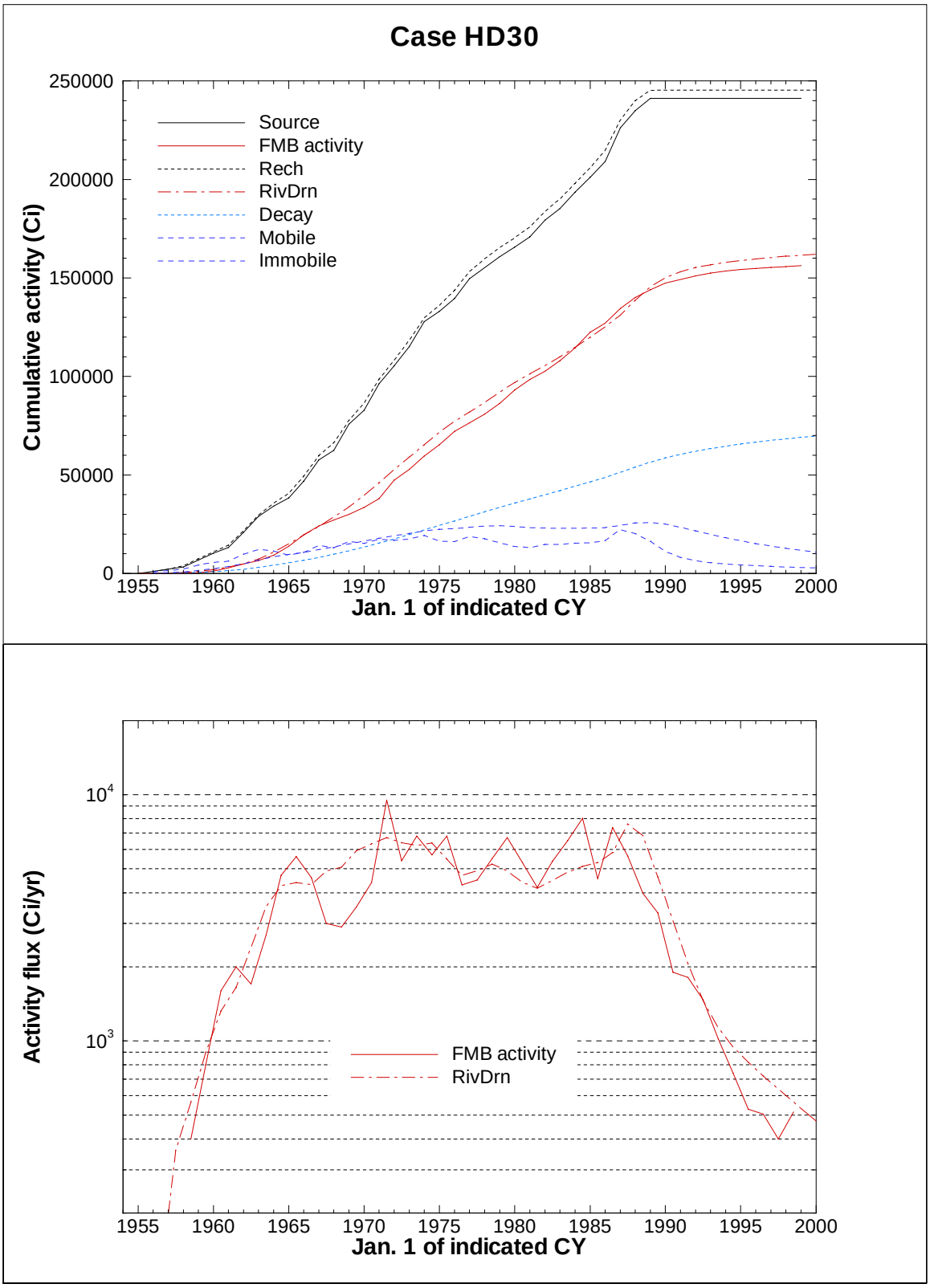

Figure 24 Calibration summary for optimal H-area dual-media transport simulation (HD-30).

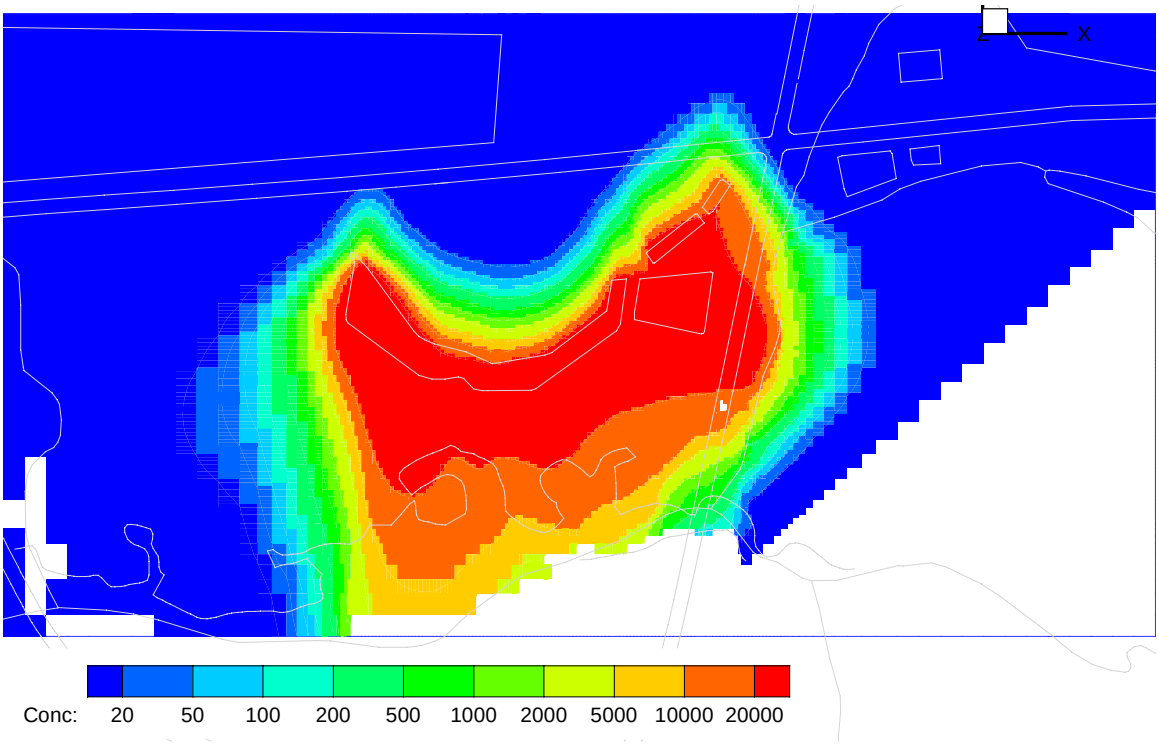

(a)

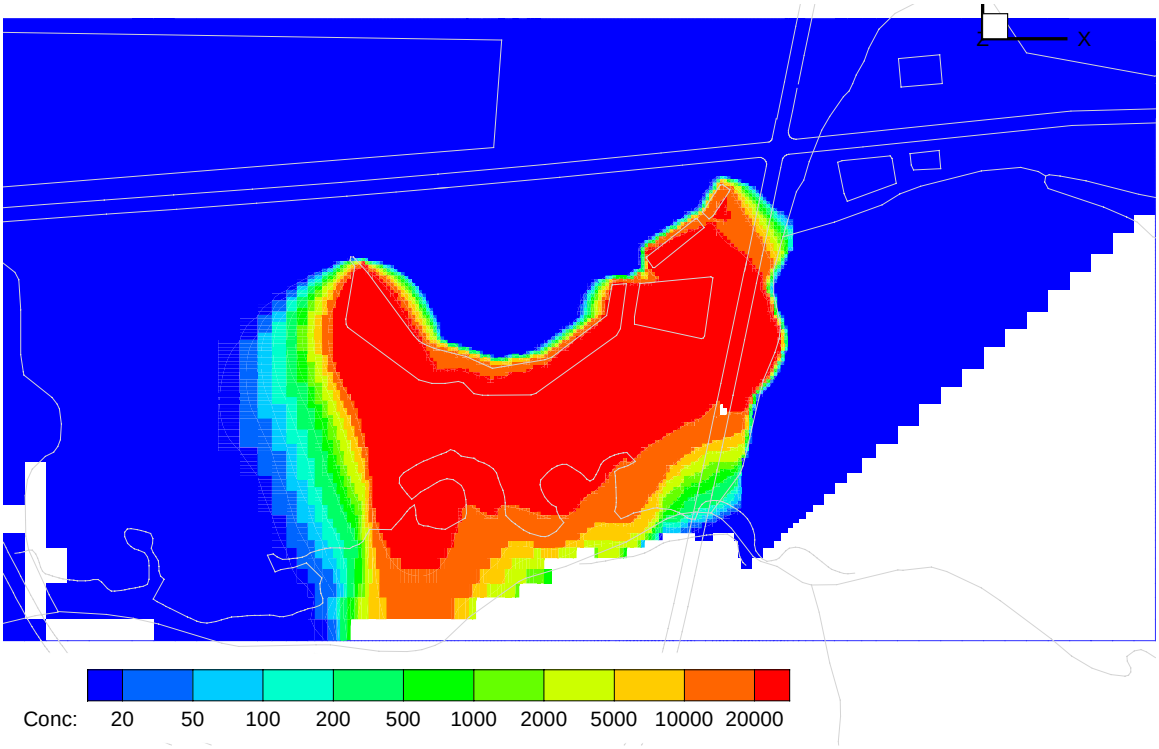

(b)

Figure 25 Comparison of simulated H-area tritium plumes in 1998 for optimal parameter settings; (a) single-medium, (b) dual-media.

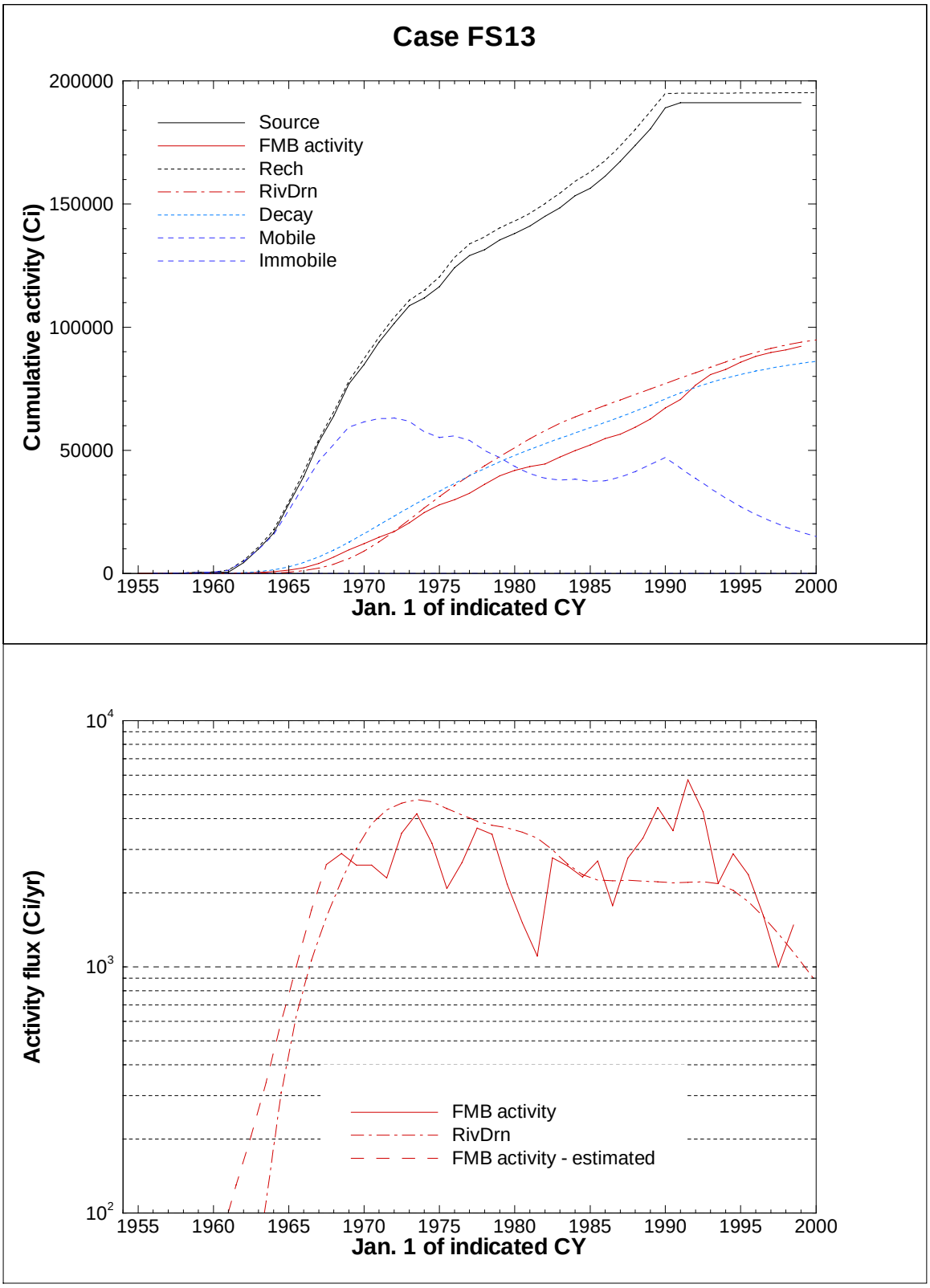

Figure 26 Calibration summary for optimal F-area single-medium transport simulation (FS-13).

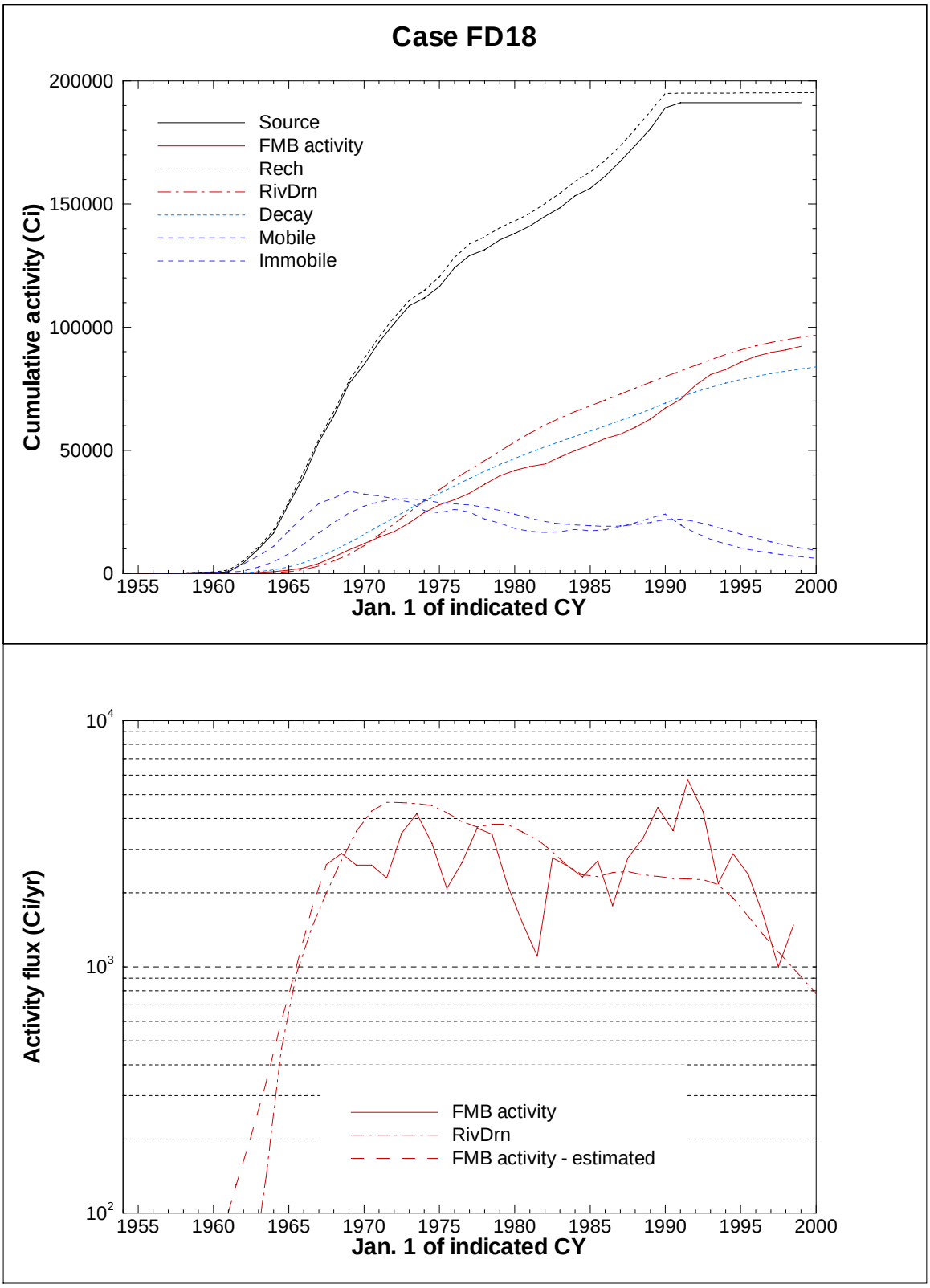

Figure 27 Calibration summary for optimal F-area dual-media transport simulation (FD-18).

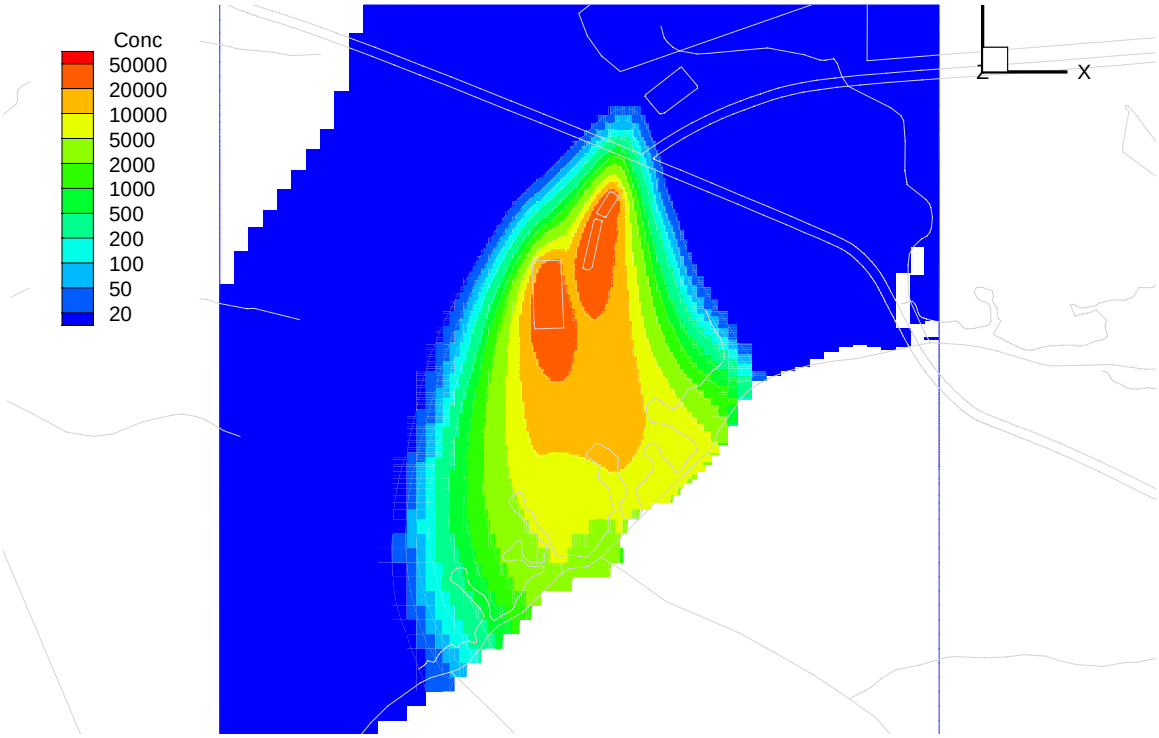

(a)

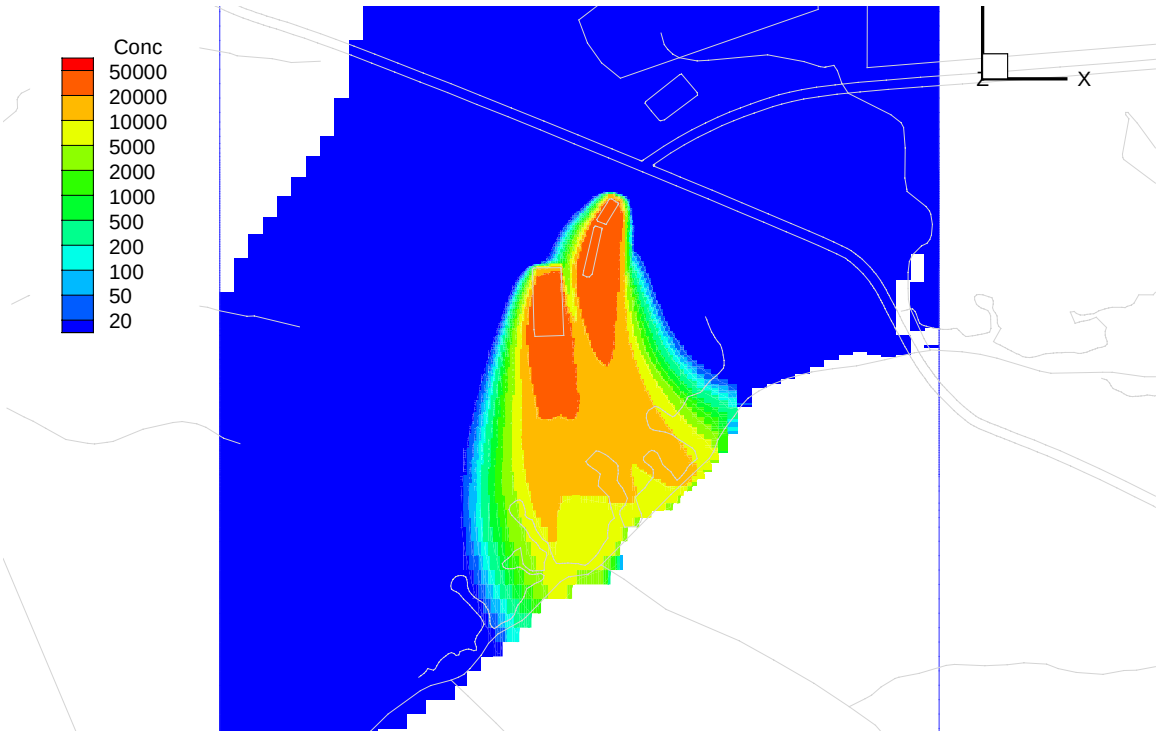

(b)

Figure 28 Comparison of simulated F-area tritium plumes in 1998 for optimal parameter settings; (a) single-medium, (b) dual-media.

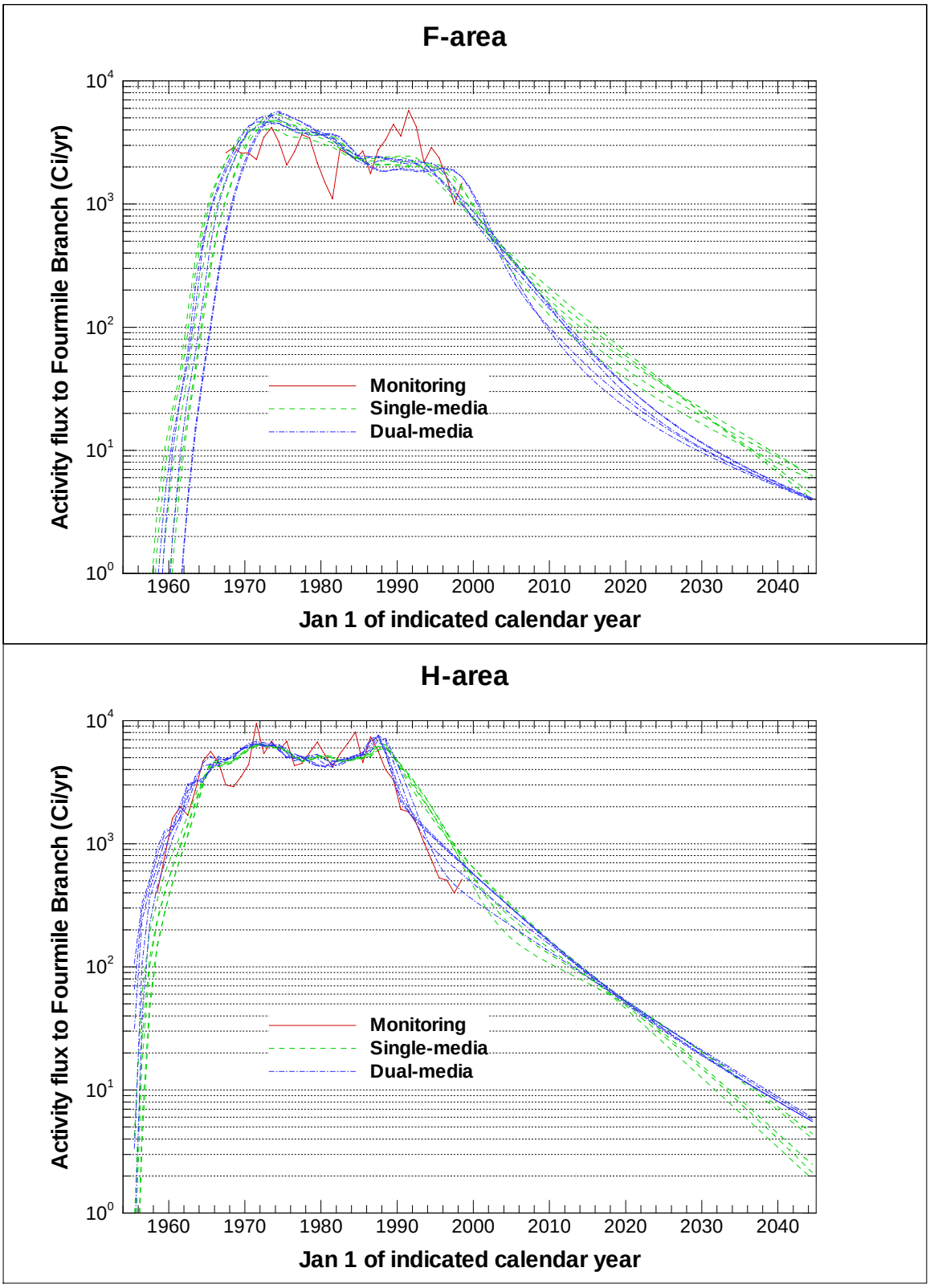

Figure 29 Breakthrough curves for 5 best single- and dual-media simulations in F- and H-area, extended to year 2050.

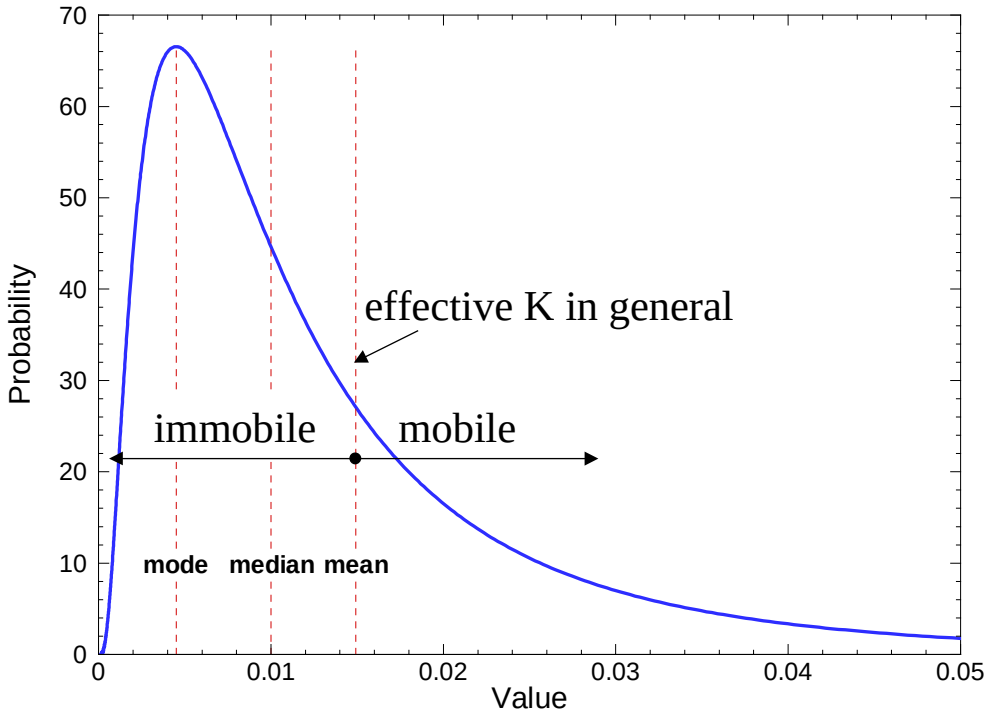

Figure 30 Concept for estimating mobile and immobile volume fractions from conductivity distribution using mean/effective conductivity cutoff.

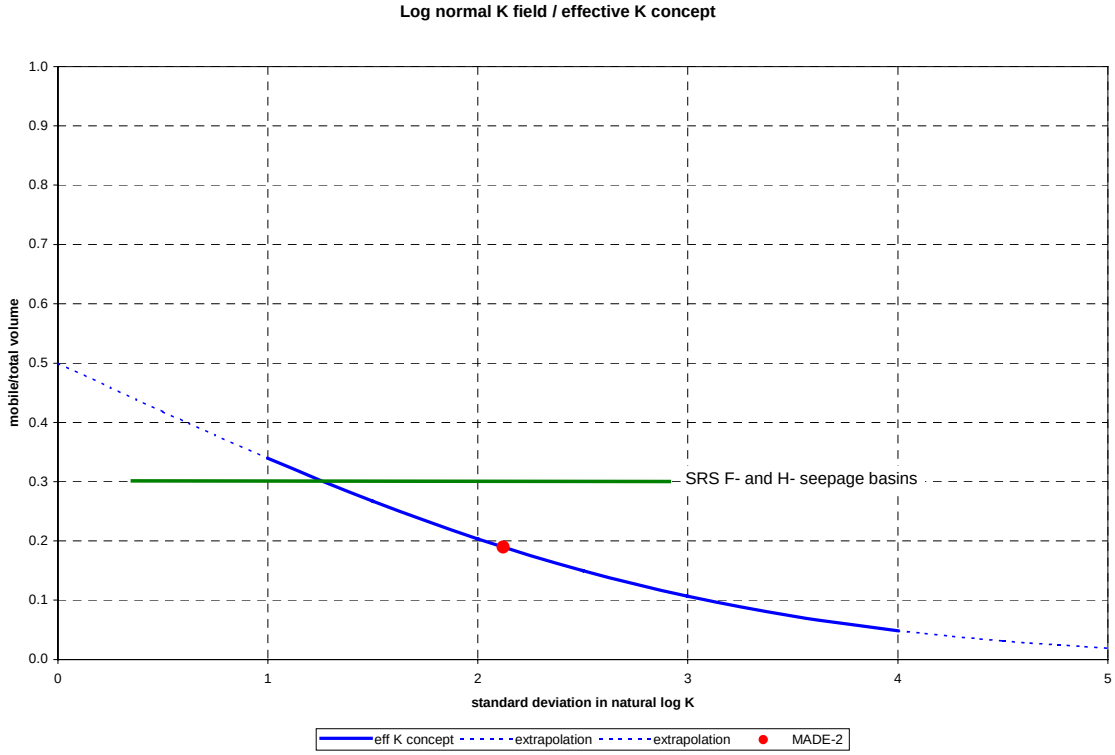

Figure 31 Mobile-immobile volume fraction estimation based on effective conductivity concept.